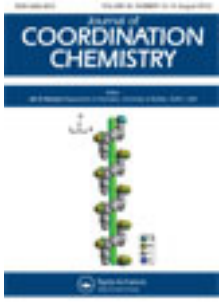

Journal of Coordination Chemistry
Publication details, including instructions for authors and subscription information:
http://www.tandfonline.com/loi/gcoo20

Synthesis, crystal structure, and properties of the cadmium complex with 2,5-bis((benzoimidazol-2-yl)methylthio)-1,3,4-thiadiazole

Yong-Hong Wen [a], Yu-Yan Chen [a], Hui-Ling Wen [a], Xing-Lei Xie [a] & Lei Wang [a]

[a] Key Laboratory of Eco-chemical Engineering, Ministry of Education, College of Chemistry and Molecular Engineering, Qingdao University of Science and Technology, Qingdao 266042, People's Republic of China

Accepted author version posted online: 19 Jun 2012.Published online: 04 Jul 2012.

To cite this article: Yong-Hong Wen, Yu-Yan Chen, Hui-Ling Wen, Xing-Lei Xie & Lei Wang (2012) Synthesis, crystal structure, and properties of the cadmium complex with 2,5-bis((benzoimidazol-2-yl)methylthio)-1,3,4-thiadiazole, Journal of Coordination Chemistry, 65:16, 2780-2792, DOI: 10.1080/00958972.2012.704549

To link to this article: http://dx.doi.org/10.1080/00958972.2012.704549

Journal of Coordination Chemistry
Vol. 65, No. 16, 20 August 2012, 2780–2792

Synthesis, crystal structure, and properties of the cadmium complex with 2,5-bis((benzoimidazol-2-yl)methylthio)-1,3,4-thiadiazole

YONG-HONG WEN*, YU-YAN CHEN, HUI-LING WEN, XING-LEI XIE and LEI WANG

Key Laboratory of Eco-chemical Engineering, Ministry of Education, College of Chemistry and Molecular Engineering, Qingdao University of Science and Technology, Qingdao 266042, People's Republic of China

(*Received 5 February 2012; in final form 7 May 2012*)

A cadmium complex, $[Cd(L)_2(CH_3OH)_2]\cdot(NO_3)_2$ (L = 2,5-bis((benzoimidazol-2-yl) methylthio)-1,3,4-thiadiazole), was synthesized and characterized by elemental analysis, infrared spectra, single-crystal and powder X-ray diffraction, UV-Vis spectra, electrochemical, and fluorescence properties. Single-crystal X-ray structure analysis reveals that the complex crystallizes in the triclinic crystal system with $P\bar{1}$ space group. The coordination geometry around cadmium is octahedral. Intermolecular hydrogen bonds result in the generation of a 1-D infinite chain structure. Both UV-Vis spectra and cyclic voltammetry studies show the Cd(II) complex could be used as a probe to distinguish ssDNA from dsDNA. Differential pulse voltammetry indicates the complex could be used to analyze quantitatively for DNA. The solid complex exhibits strong luminescence emission in the visible region at room temperature upon excitation with UV radiation.

Keywords: Benzimidazole; Cadmium complex; Crystal structure; Fluorescence; Electrochemical property

1. Introduction

Benzimidazole-containing compounds have attracted attention since the first benzimidazole compound, 2,5-dimethylbenzimidazole, was synthesized in 1872 [1, 2]. Benzimidazole-containing complexes with transition metals is one of the most important subjects in coordination chemistry, crystal engineering, medicine and materials science owing to their structural motifs [3] and characteristic properties such as catalysis [4], luminescence [5–7], antivirus activity [8, 9], and electrochemical properties [10]. Cu complexes of 1,1′-(1,5-pentanediyl)bis1*H*-benzimidazole) are efficient homogeneous catalysts for oxidative coupling of 2,6-dimethylphenol [4]. Co complex of 2-(2-pyridyl) benzimidazole has been used as an efficient fluorescent probe for trace determination of aspartic and glutamic acids [7]. Cu and Cd complexes of

*Corresponding author. Email: yonghwen@163.com; inorchemwl@126.com

ISSN 0095-8972 print/ISSN 1029-0389 online
http://dx.doi.org/10.1080/00958972.2012.704549

several bis(benzimidazole) ligands have been examined as potential models of structure and mobility of biological metal binding sites [3].

1,3,4-Thiadiazole and its derivatives are used in pharmaceutical [11] and coordination chemistry [12, 13]. Benzimidazole and 1,3,4-thiadiazole are both inexpensive and have large planar π-conjugated systems. However, compounds containing both benzimidazole and 1,3,4-thiadiazole have not been investigated. As part of our ongoing work on the syntheses and properties of benzimidazole-containing complexes [14], a new thiodiazole-based bis(benzimidazole), 2,5-bis((benzoimidazol-2-yl)methylthio)-1,3,4-thiadiazole (**L**), was synthesized and reacted with $Cd(NO_3)_2$, giving a new coordination compound, $[Cd(L)_2(CH_3OH)_2] \cdot (NO_3)_2$, which was characterized by elemental analysis, infrared (IR) spectra, single-crystal X-ray diffraction, powder X-ray diffraction, ultraviolet and visible spectra (UV-Vis), electrochemical, and fluorescence properties.

2. Experimental

2.1. *Materials and measurements*

All commercially available reagents and chemicals were of analytical grade purity and used without purification. Salmon sperm DNA was purchased from Shanghai Huashun biological Engineering Company. Deionized water was obtained by passing distilled water through a Barnstead E-pure 3-Module system. C, H, N, and S contents were determined using an Elementar Vario EL III analyzer. IR spectra were recorded from KBr pellets by a Nicolet 510P FT-IR spectrometer. NMR spectra were recorded on a Bruker Avance 500 MHz spectrometer with TMS as an internal standard. Conductivity measurement was carried out with a DDS-11A type conductometer for 1.0×10^{-3} mol L^{-1} solution in DMF at 25°C. Ultraviolet and visible spectra (UV-Vis) spectra were measured using a Cary 500 UV-Vis-NIR spectrophotometer. Fluorescence spectra were measured using a HITACHI F-4500 fluorescence spectrophotometer. Powder X-ray diffraction (XRD) patterns were recorded (Bragg-Brentano) on a Siemens D5005 diffractometer using Cu-Kα radiation ($\lambda = 1.5418$ Å) with a graphite monochromator. The step size was 0.02° and the count time was 4 s.

2.2. *Synthesis*

2.2.1. Synthesis of 2,5-bis((benzoimidazol-2-yl)methylthio)-1,3,4-thiadiazole (L). 2-Chloromethylbenzoimidazole was synthesized by refluxing a solution of benzene-1,2-diamine, 2-chloroacetic acid and 5 mol L^{-1} hydrochloride for 4 h, followed by adjusting the pH to 8–9 with ammonia. After stirring the 50 mL acetone solution of 2,5-dimercapto-1,3,4-thiodiazole (3.00 g, 20 mmol), K_2CO_3 (3.05 g, 22 mmol), and KI (0.5 g) at room temperature for 30 min, a 30 mL solution of 2-chloromethylbenzoimidazole (6.67 g, 40 mmol) in acetone was added dropwise, and the mixture was refluxed for 4 h. After cooling to room temperature, the mixture was washed three times with water (3×6 mL) and then filtered. The resulting solid was washed three times with acetone (3×6 mL) to obtain a crude product. Recrystallization of the crude product in EtOH/DMF (1 : 1) afforded **L** as yellow crystals. Yield: 72.8%. ^{1}H NMR (500 MHz, DMSO-d_6, δ (ppm)): 12.58 (s, 1 H, NH), 7.51–7.53 (m, 2H, ArH), 7.16–7.17

(m, 2H, ArH), 4.76 (s, 2H, CH_2); ^{13}C NMR (125 MHz, DMSO-d_6, δ (ppm)): 165.17 (1C, C of thiadiazole ring), 149.88 (1C, C in 2-position of imidazole ring), 139.06 (2C), 122.34 (2C), 115.05 (2C), (C of benzene ring), 31.72 (CH_2). IR (KBr pellet, cm^{-1}): 3428s, 3248m, 2920w, 1666m, 1626w, 1531w, 1487w, 1439m, 1396m, 1381m, 1313w, 1273m, 1225w, 1151w, 1050m, 854w, 749w, 737m, 621w. Anal. Calcd for $C_{18}H_{14}N_6S_3$: C, 52.66; H, 3.44; N, 20.47; S, 23.43. Found: C, 52.34; H, 3.26; N, 20.15; S, 23.34.

2.2.2. Synthesis of $[Cd(L)_2(CH_3OH)_2]\cdot(NO_3)_2$. A solution of $Cd(NO_3)_2\cdot 4H_2O$ (0.0771 g, 0.25 mmol) in 12 mL methanol was added dropwise with stirring to a solution of **L** (0.2052 g, 0.5 mmol) in 15 mL methanol. The resulting mixture was stirred at room temperature for 6 h. The precipitate was filtered, washed with methanol, and dried *in vacuo* over P_2O_5 for 48 h. Yield: 0.2017 g, 72%. IR data (KBr pellet, cm^{-1}): 3428 sb, 3057w, 2929w, 2854w, 2767w, 1622w, 1527w, 1485w, 1444s, 1431s, 1384s, 1313w, 1276m, 1239w, 1152w, 1047m, 1007w, 912w, 862w, 742 s, 708w, 663w, 636w. Anal. Calcd for $C_{38}H_{36}N_{14}O_8S_6Cd$: C, 40.69; H, 3.24; N, 17.48; S, 17.15. Found: C, 40.37; H, 3.09; N, 17.59; S, 17.26. Colorless column crystals suitable for X-ray diffraction analysis were obtained by slow evaporation of a DMSO-methanol (1 : 2, v/v) solution of the solid complex for 30 days.

2.3. *X-ray crystallography*

Single-crystal X-ray diffraction data were collected by a Bruker SMART 1000 CCD diffactometer with graphite monochromated Mo-Kα radiation ($\lambda = 0.71073$ Å) using ω scan mode at 113(2) K. Intensity data were corrected for *Lp* factors and empirical absorption. The structure was solved by direct methods and expanded by Fourier differential techniques with SHELXTL [15]. All non-hydrogen atoms were located with successive difference Fourier syntheses. Hydrogen atoms were geometrically fixed and allowed to ride on the parent to which they are attached. The structure was refined by full-matrix least-squares on F^2 with anisotropic thermal parameters for all non-hydrogen atoms. Atomic scattering factors and anomalous dispersion corrections were taken from International tables for X-ray crystallography [16]. A summary of the key crystallographic data and structural refinements for the complex is presented in table 1. Selected bond distances and angles are illustrated in table 2.

2.4. *Electrochemical studies*

All electrochemical experiments were performed with a CHI 832B electrochemical analyzer (Shanghai CHI Instrument Company, China) using a three-electrode system composed of a glassy carbon electrode (GCE, $\varphi = 2.96$ mm) as a working electrode, Ag/AgCl/(saturated)KCl as a reference electrode, and Pt wire as an auxiliary electrode. A 0.2 mol L^{-1} Britton–Robinson buffer solution (BR buffer, the mixture of 3.39 mL 85% H_3PO_4, 2.95 mL HOAc and 3.0875 g H_3BO_3 diluted to 250 mL, and adjusted to pH 4.0 with 0.5 mol L^{-1} NaOH) was used as buffer solution. The pH was measured with a PHS-3D pH-meter (Shanghai LeiCi Device Works, Shanghai, China) with a combined glass-calomel electrode. Cyclic voltammetry measurements were made on a glassy carbon electrode in BR buffer (pH 5.0) at room temperature with scan rates

Table 1. Crystal data and structure refinement of complex.

Empirical formula	$C_{38}H_{36}CdN_{14}O_8S_6$
Formula weight	1121.64
Crystal system	Triclinic
Space group	$P\bar{1}$
Temperature (K)	113(2)
Unit cell dimensions (Å, °)	
a	9.0931(2)
b	11.189(2)
c	11.255(2)
α	95.48(3)
β	92.98(3)
γ	91.96(3)
Volume (Å^3), Z	1137.5(4), 1
Calculated density (g cm^{-3})	1.637
Absorption coefficient (mm^{-1})	0.823
Crystal size (mm^3)	$0.12 \times 0.10 \times 0.04$
θ range for data collection (°)	1.82 – 25.02
Reflections collected	6498
Independent reflection	3942
Data/parameters	3942/311
Goodness-of-fit on F^2	1.001
R indices (all data)	$R^a = 0.0534$, $wR^b = 0.1181$
Final R indices [$I > 2\sigma(I)$]	$R^a = 0.0499$, $wR^b = 0.1150$

[a] $R = \sum||F_o| - |F_c||/\sum|F_o|$; [b] $wR = [\sum w(F_o^2 - F_c^2)/\sum w(F_o^2)^2]^{1/2}$.

Table 2. Selected bond lengths (Å) and angles (°) for complex.

Cd(1)–N(1)	2.247(4)	Cd(1)–N(1A)[a]	2.247(4)
Cd(1)–O(1)	2.347(3)	Cd(1)–O(1A)[a]	2.347(3)
Cd(1)–N(3)	2.407(4)	Cd(1)–N(3A)[a]	2.407(4)
N(1)–Cd(1)–O(1)	91.36(12)	N(1A)[a]–Cd(1)–O(1A)[a]	91.36(12)
N(1)–Cd(1)–O(1A)[a]	88.64(12)	N(1A)[a]–Cd(1)–O(1)	88.64(12)
N(1)–Cd(1)–N(3)	87.08(13)	N(1A)[a]–Cd(1)–N(3)[a]	87.08(13)
N(1)–Cd(1)–N(3A)[a]	92.92(13)	N(1A)[a]–Cd(1)–N(3)	92.92(13)
O(1A)[a]–Cd(1)–N(3)	97.72(12)	O(1)–Cd(1)–N(3A)[a]	97.72(12)
O(1)–Cd(1)–N(3)	82.28(12)	O(1A)[a]–Cd(1)–N(3A)[a]	82.28(12)
N(1)–Cd(1)–N(1A)[a]	180.00(1)	O(1)–Cd(1)–O(1A)[a]	180.00(1)
N(3)–Cd(1)–N(3A)[a]	180.00(1)		

Symmetry code: [a] $1 - x$, $1 - y$, $1 - z$.

of 20–200 mV s^{-1}. The GCE was polished successively with 0.3 and 0.05 μm Al_2O_3 slurry on emery paper. It was then rinsed with doubly-distilled water and sonicated in 1 mol L^{-1} HNO_3, acetone and doubly-distilled water for 10 min. Solutions of complex was prepared by dissolution in appropriate amount of DMSO and then mixing in B–R buffer.

3. Results and discussion

3.1. *IR Spectral studies*

When the IR spectrum of free ligand is contrasted with that of complex, the difference is apparent. In the IR spectrum of complex, there is a broad band at 3428 cm^{-1} for O–H

stretch of methanol, thus indicating the presence of methanol. The strong absorption at 1384 cm^{-1} is assignable to uncoordinated nitrate [17]. These are in good agreement with the result of the single-crystal structure analysis.

3.2. *X-ray crystal structure of complex*

Single-crystal X-ray diffraction analysis reveals that the crystal structure of the complex is composed of $[Cd(L)_2(CH_3OH)_2]^{2+}$ and two NO_3^-'s linked by hydrogen bonds and *van der Waals*' forces. The molecular structure of the complex with the atom numbering scheme is shown in figure 1. The complex crystallizes in the triclinic space group $P\bar{1}$ with half a molecule per asymmetric unit. The other half of the molecule is generated from the first one by the crystallographic inversion centre. The Cd(II) is six-coordinate with four nitrogen atoms from two **L**'s and two oxygen atoms from two methanols. All coordinated bond lengths (table 2) show normal values and are comparable to those in related benzimidazole and 1,3,4-thiadiazole compounds [14, 18–21]. The coordination geometry around Cd is best described as octahedral (figure S1 in Supplementary Material). The equatorial positions are occupied by N(1), O(1), N(1A), and O(1A) with the sum of the angles N(1)–Cd(1)–O(1), N(1A)–Cd(1)–O(1), N(1A)–Cd(1)–O(1A), and N(1)–Cd(1)–O(1A) being 360°, and the axial positions by N(3) and N(3A) with N(3)–Cd(1)–N(3A) angle being 180(1)°.

L is a bidentate ligand to form a stable seven-membered ring, leaving one benzimidazole uncoordinated. The thiadiazole and benzimidazole rings are

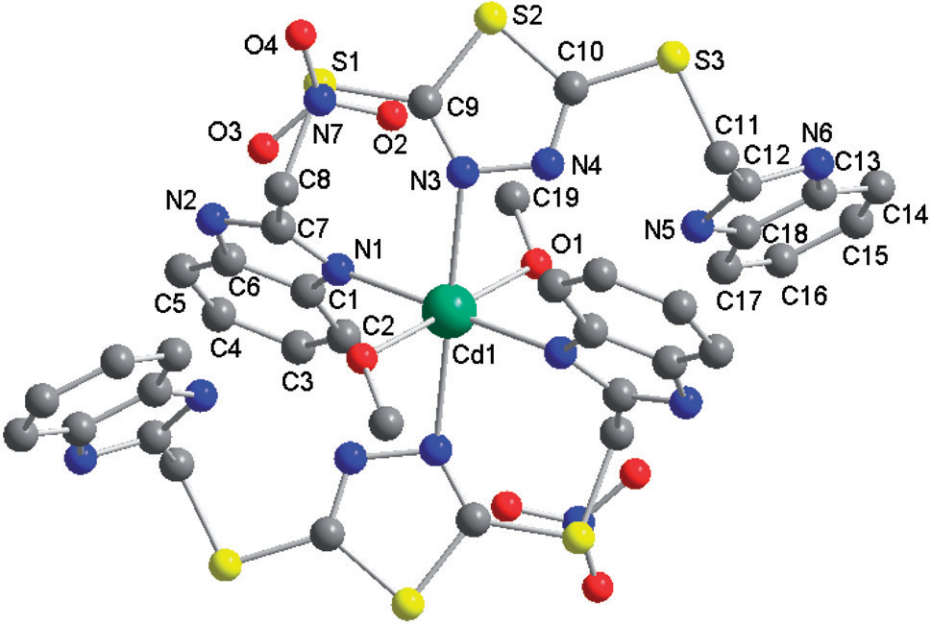

Figure 1. The molecular structure of the complex showing the atom-labeling scheme. Hydrogen atoms are omitted for clarity. The unlabelled atoms are related to the labeled atoms by the symmetry operator $(1-x, 1-y, 1-z)$.

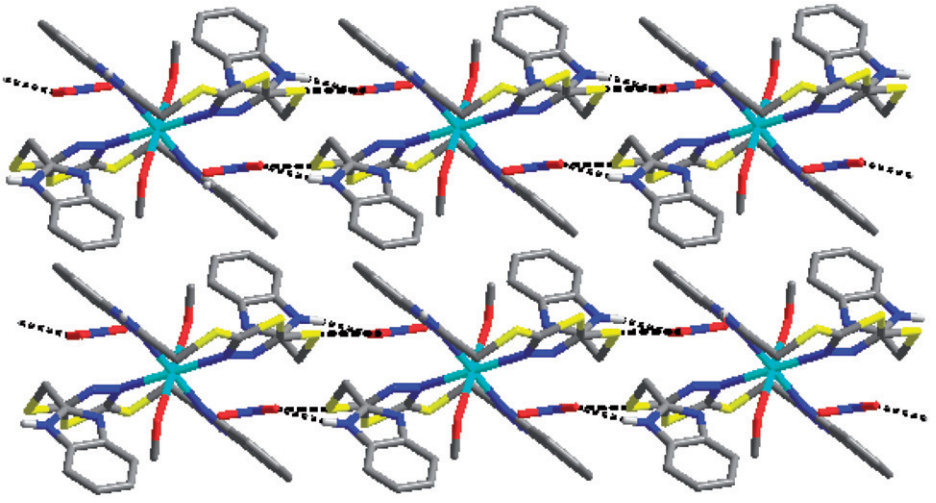

Figure 2. The 1-D infinite chain structure of complex, formed by hydrogen bonds of nitrates, viewed down the *b* axis.

Table 3. Hydrogen bond data (Å) and (°) for complex.

D–H···A	*d*(D–H)	*d*(H···A)	*d*(D···A)	∠DHA
O(1)–H(1)···N(5)	0.93	2.15	2.744(4)	121
N(2)–H(2)···O(3)[a]	0.86	2.00	2.822(5)	161
N(2)–H(2)···O(4)[a]	0.86	2.47	3.012(5)	121
N(6)–H(6)···O(4)[b]	0.86	1.94	2.793(5)	171
C(8)–H(8B)···N(3)	0.97	2.58	2.963(6)	104
C(8)–H(8B)···O(1)[c]	0.97	2.38	3.194(5)	141
C(11)–H(11A)···N(4)	0.97	2.36	2.842(6)	110

Symmetry codes: [a]$1-x,-y,1-z$; [b]$1-x,1-y,2-z$; [c]$1-x,1-y,1-z$.

essentially planar. The dihedral angles between thiadiazole and two benzimidazole rings are 66.2(2)° and 72.9(2)°, respectively. The two nitrates are not coordinated and balance the charge.

There are different types of hydrogen bonds in the complex. Nitrates form intermolecular hydrogen bonds, N(2)–H(2)···O(3), N(2)–H(2)···O(4), and N(6)–H(6)···O(4), connecting the complex into infinite chains (figure 2 and table 3). Methanol as hydrogen bond donors form intramolecular O(1)–H(1)···N(5) hydrogen bonds with uncoordinate benzimidazole (figure 2 and table 3). Finally, there exist different types of C–H···O and C–H···N hydrogen bonds in the complex (table 3). The crystal structure is stabilized by these hydrogen bond interactions.

3.3. *Powder X-ray diffraction and molar conductivity*

The experimental powder X-ray diffraction pattern is in good agreement with the simulated one on the basis of the single-crystal structure (figure S2 in Supplementary material), suggesting phase purity of the synthesized sample.

Molar conductivity of the complex in DMF at 25°C is 151 S cm^2 mol^{-1}, indicating that the complex is a 1 : 2 electrolyte and two nitrates are out of the coordination sphere [22]. This agrees with the results of the spectral studies and single-crystal structure analysis.

3.4. *UV-Vis absorption spectra studies*

Electronic absorption spectra of ligand and complex were recorded from 200 to 700 nm with clear difference between the absorption spectra of ligand (curve a in figure 3) and complex (curve b in figure 3), showing the formation of complex. In the absorption spectrum of ligand (curve a in figure 3), the strong absorption at 276 nm and the broad shoulder lower than 255 nm could be assigned to benzimidazole and thiadiazole intraligand $\pi\rightarrow\pi^*$ transitions, respectively. In the absorption spectrum of complex, a new absorption at 270 nm was observed from one benzimidazole ring coordinated to Cd(II) and the broad shoulder lower than 255 nm became an absorption at 242 nm from thiadiazole ring coordinated to Cd(II) (see crystal structure section). The absorption spectrum of complex (curve c in figure 3) had little change after adding dsDNA to the solution, while the absorption spectrum of complex (curve d in figure 3) had obvious decrease after adding the same concentration ssDNA. Absorptions had no red shift, suggesting that the interaction between Cd(II) and DNA might be electrostatic [23]. The hypochromic effect by ssDNA shows the Cd(II) complex could be a probe for recognition of ssDNA from dsDNA.

DNA binding of Cd(II) complex was studied by UV-Vis titration. For the UV-Vis titration experiment, 20 µL solutions of DNA (7.0×10^{-4} mol L^{-1} in water) were added to a 2.5 mL solution of Cd(II) complex (5.05×10^{-5} mol L^{-1} in water) by a micropipette. Because of the limited solubility of the complex in water, the titration experiments were carried out in the presence of a small amount of DMSO. The intrinsic binding constant K_b was evaluated from the collected absorbance data of the titration curve at the specified wavelength and the following equation [24],

$$C_{DNA}/(\varepsilon_a-\varepsilon_f)=C_{DNA}/(\varepsilon_b-\varepsilon_f)+1/K_b(\varepsilon_b-\varepsilon_f)$$

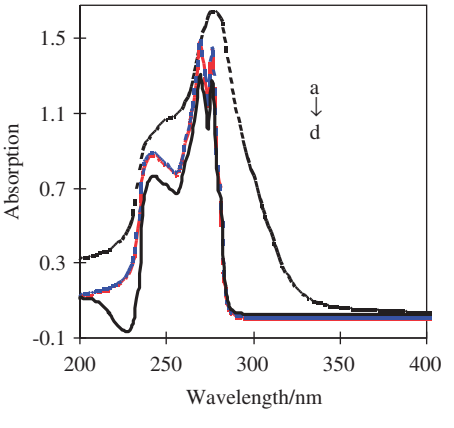

Figure 3. UV-Vis absorption spectra: (a) 1.01×10^{-4} mol L^{-1} ligand; (b) 5.05×10^{-5} mol L^{-1} complex; (c) b + 8.4×10^{-6} mol L^{-1} dsDNA; and (d) b + 8.4×10^{-6} mol L^{-1} ssDNA.

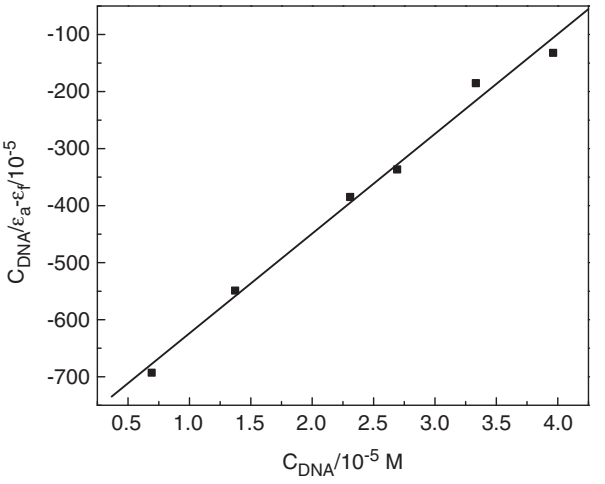

Figure 4. Plot of $C_{DNA}/(\varepsilon_a - \varepsilon_f)$ against C_{DNA}.

where C_{DNA} is the concentration of DNA, ε_f, ε_a, and ε_b refer to the extinction coefficients for the free complex, for each addition of DNA to the complex and for thecomplex in the fully bound form, respectively. When $C_{DNA}/(\varepsilon_a - \varepsilon_f)$ is plotted against C_{DNA}, a straight line is obtained (figure 4). The binding constant K_b obtained by the ratio of the slope to the intercept is $2.19 \times 10^4\,L\,mol^{-1}$. This K_b value is comparable to those of the related bisbenzimidazole cadmium(II) complexes ($2.3 \times 10^4\,L\,mol^{-1}$ for $[Cd(L)_2] \cdot (pic)_2$ (L = 1,3-bis((1-ethylbenzimidazol-2-yl)-2-thiapropane) [25] and $1.42 \times 10^5\,L\,mol^{-1}$ for $[Cd(L)Br_2]$ (L = 1,3-bis((1-benzylbenzimidazol-2-yl)-2-thiapropane)) [26], but much higher than that of histidine cadmium(II) complex ($4.56 \times 10^2\,L\,mol^{-1}$ for $[Cd(HL)_2] \cdot H_2O$ (H_2L = *N*-(2-hydroxybenzyl)-L-histidine) [27]. Different structures may cause different binding affinity with DNA.

3.5. *Electrochemical studies*

The electrochemical behavior of the complex in the absence and presence of DNA was studied by cyclic voltammograms in 5 mL 0.04 mol L^{-1} BR buffer solution (pH 5.0) containing 1.003×10^{-4} mol L^{-1} Cd complex.

As shown in figure 5 (curve a), the Cd(II) complex shows a pair of redox peaks with a cathodic peak potential (E_{pc}) at 0.200 V and an anodic peak potential (E_{pa}) at 0.319 V. The formal potential ($E_{1/2} = 1/2(E_{pa} + E_{pc})$), the peak-to-peak potential separation (ΔE_p), and the ratio of peak current (I_{pa}/I_{pc}) were obtained as 0.259 V, 0.119 V, and 3.75, respectively, indicating that the electrochemical behavior of Cd(II) complex is irreversible [28].

Curves b and c in figure 5 were the voltammograms when Cd(II) complex interacted with the same concentration dsDNA and ssDNA, respectively. In the presence of DNA, the cyclic voltammograms exhibited significant decrease in peak current, but little shift in formal potential. $E_{1/2}$, ΔE_p, and I_{pa}/I_{pc} were obtained as 0.259, 0.103, and 4.90 V for dsDNA, and 0.259, 0.101 and 4.22 V for ssDNA, respectively, indicating the interaction between the complex and the DNA. The decrease in the voltammetric currents in the

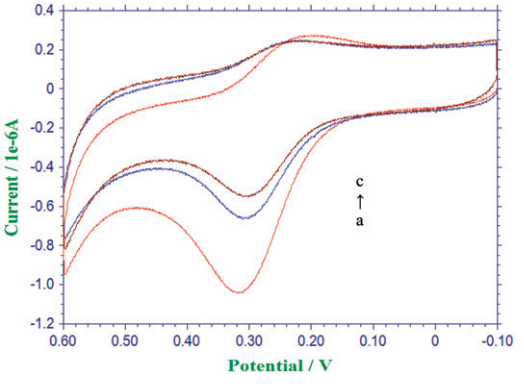

Figure 5. Cyclic voltammograms of Cd complex in the absence (a) and presence of dsDNA (b) and ssDNA (c). (a): 1.003×10^{-4} mol L^{-1} complex + 0.04 mol L^{-1} B–R buffer solution (pH = 5.0); (b): (a) + 2.1×10^{-5} mol L^{-1} dsDNA; (c): (a) + 2.1×10^{-5} mol L^{-1} ssDNA.

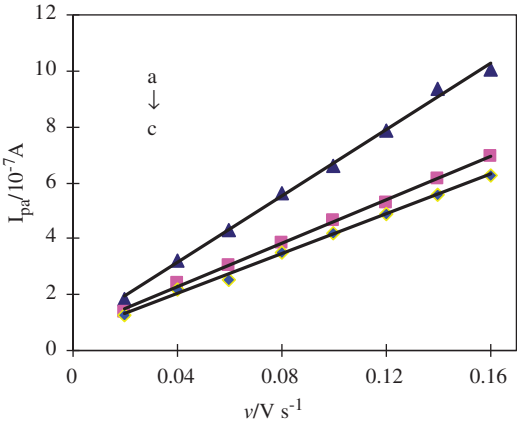

Figure 6. Plot of peak current (I_{pa}) against scan rate (v). (a): Complex, (b): (a) + dsDNA, (c): (a) + ssDNA.

presence of DNA can be attributed to slow diffusion of the complex bound to the large, slowly diffusing DNA, and the unchanged formal potentials are probably because the oxidation state and the reduction state of complex could interact with DNA to the same degree [29–31]. Interaction between Cd(II) complex and ssDNA is stronger than that between Cd(II) complex and dsDNA (figure 5) because of the exposed bases of ssDNA [32], consistent with the absorption spectra results.

The effect of varying the potential scan rate (v) on the oxidation peak current was also examined. The results showed that oxidation peak currents of Cd complex increased linearly with scan rate in the absence and presence of DNA over the range 0.02–0.16 V s^{-1} (figure 6), suggesting that the oxidation of complex at the CPE is adsorption-controlled. The decrease in slopes of straight lines in the presence of DNA indicates the decrease in diffusion coefficient [33].

For adsorption-controlled and irreversible electrode process, according to Laviron [34], the oxidation peak potential (E_p) can be described by the following equation:

$$E_p = E^{0'} + (RT/\alpha nF)\ln(RTk^0/\alpha nF) + (RT/\alpha nF)\ln v$$

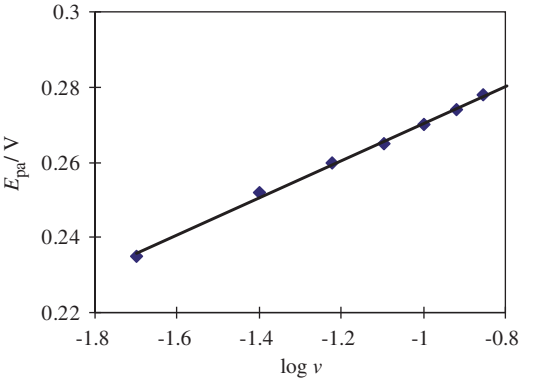

Figure 7. Plot of oxidation peak potential (E_p) against log v.

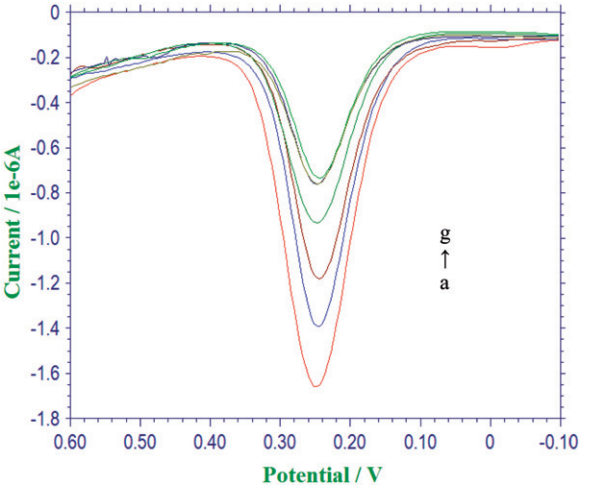

Figure 8. Differential pulse voltammograms of the complex (1.003×10^{-4} mol L^{-1}) in 0.04 mol L^{-1} B–R buffer solution (pH = 5.0) varying concentration of dsDNA (10^{-6} mol L^{-1}), (a) 0, (b) 3.4826, (c) 6.9625, (d) 10.448, (e) 13.931, (f) 17.413, and (g) 20.895.

where $E^{0'}$ is the formal potential, T is the temperature, α is the transfer coefficient, n is the number of electrons transferred in the rate-determining step, k^0 is the electrochemical rate constant, and F is the Faraday constant. The relationship between E_p and v was investigated and E_p depends linearly on the logarithm of v according to the equation $E_p = 0.0493 \log v + 0.3196$ with a correlation coefficient of 0.9977 (figure 7). The value of αn, calculated from the slope of 0.0493, is 1.1658. Generally, α is assumed to be 0.5 in a totally irreversible electrode process. Thus, two electrons are involved in the oxidation of complex.

Differential pulse voltammograms of the complex with varying concentration of dsDNA are shown in figure 8. The oxidation peak current decreased with increase in concentration of dsDNA. The oxidation peak current was constant when the concentration of dsDNA is 1.393×10^{-5} mol L^{-1}, showing the complex in the fully bound form. When ΔI_{pa} is plotted against C_{DNA}, a straight line is obtained (figure 9),

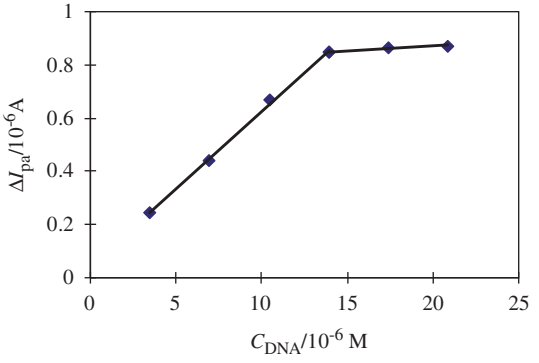

Figure 9. Plot of ΔI_{pa} against C_{DNA}.

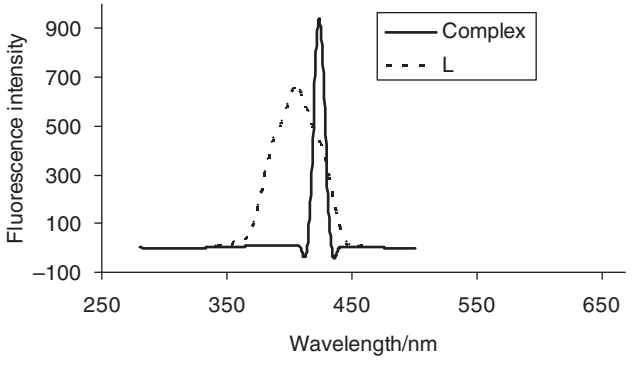

Figure 10. Fluorescence emission spectra of **L** (dot) and complex (solid) in solid state at room temperature.

indicating the complex could be used to analyze quantitatively DNA over the range $3.4826 \times 10^{-6} - 1.393 \times 10^{-5}$ mol L^{-1}.

3.6. *Fluorescent properties*

The solid-state fluorescence of **L** and complex were investigated at room temperature (figure 10). **L** displays an intense fluorescence emission maximum at 407 nm when excited at 320 nm, assigned to the intraligand (π–π*) fluorescent emission. At the same conditions, the complex exhibits more intense fluorescence with an emission maximum at 424 nm upon excitation at 350 nm, red-shifted 17 nm with respect to free ligand. Enhancement of fluorescence in complex with d^{10} configuration may be attributed to coordination of ligand to cadmium [35]. The coordination increases rigidity of ligand, as indicated in X-ray diffraction analysis, and thus reduces the loss of energy through a radiationless pathway. The red shift of the emission of complex is attributed to ligand-to-metal charge transfer, which has been found in similar Cd coordination compounds [36–38]. The strong and narrow fluorescence emission suggests the complex can be used as a potential optical material.

4. Conclusion

A new thiodiazole-based bis(benzimidazole), 2,5-bis((benzoimidazol-2-yl)methylthio) 1,3,4-thiadiazole (L), and its cadmium complex, $[Cd(L)_2(CH_3OH)_2]\cdot(NO_3)_2$, were synthesized and characterized. The coordination geometry is octahedral. Intermolecular hydrogen bonds in the complex result in generation of a 1-D chain. Both UV-Vis spectra and cyclic voltammetry studies show that interaction between Cd(II) complex and ssDNA is stronger than that with dsDNA, indicating the Cd(II) complex could be used as a probe to distinguish ssDNA from dsDNA. The interaction of Cd(II) complex with salmon sperm DNA might be electrostatic binding. Differential pulse voltammetry indicates the complex could be used to analyze quantitatively DNA. The solid complex exhibits strong luminescence emission in the visible region at room temperature upon excitation with UV radiation, suggesting the complex could be a potential fluorescent material.

Supplementary material

Crystallographic data for the structural analyses of complex has been deposited with the Cambridge Crystallographic Data Center (CCDC). CCDC reference number 865269 contains the supplementary crystallographic data for this article. These data can be obtained free of charge from The Cambridge Crystallographic Data Centre *via* www.ccdc.cam.ac.uk/data_request/cif

Acknowledgments

This work was supported by the National Natural Science Foundation of China (No. 20971076) and the Science and Technology Projects (Nos. BS2010NJ004, 2009ZRB019KH) of Shandong Province, China.

References

[1] F. Hobrecker. *Ber. Dtsch. Chem. Ges.*, **5**, 920 (1872).
[2] J.B. Wright. *Chem. Rev.*, **48**, 397 (1951).
[3] J.C. Lockhart, W. Clegg, M.N.S. Hill, D.J. Rushton. *J. Chem. Soc., Dalton Trans.*, 3541 (1990).
[4] B. Xiao, H. Hou, Y.J. Fan. *Organomet. Chem.*, **692**, 2014 (2007).
[5] L. Ma, Y.C. Qiu, G. Peng, J.B. Cai, H. Deng, M. Zeller. *CrystEngComm*, **13**, 3852 (2011).
[6] Q.-D. Liu, W.-L. Jia, S. Wang. *Inorg. Chem.*, **44**, 1332 (2005).
[7] S. Das, S. Guha, A. Banerjee, S. Lohar, A. Sahana, D. Das. *Org. Biomol. Chem.*, **9**, 7097 (2011).
[8] N.M. Salunke, V.K. Revankar, V.B. Mahale. *Transition Met. Chem.*, **19**, 53 (1994).
[9] Y.-F. Li, G.-F. Wang, P.-L. He, W.-G. Huang, F.-H. Zhu, H.-Y. Gao, W. Tang, Y. Luo, C.-L. Feng, L.-P. Shi, Y.-D. Ren, W. Lu, J.-P. Zuo. *J. Med. Chem.*, **49**, 4790 (2006).
[10] R.T. Stibrany, M.V. Lobanov, H.J. Schugar, J.A. Potenza. *Inorg. Chem.*, **43**, 1472 (2004).
[11] A. Demirbas, D. Sahin, N. Demirbas, S.A. Karaoglu. *Eur. J. Med. Chem.*, **44**, 2896 (2009).
[12] Z. Huang, M. Du, H.-B. Song, X.-H. Bu. *Cryst. Growth Des.*, **4**, 71 (2004).
[13] J.-L. Song, Z.-C. Dong, H.-Y. Zeng, W.-B. Zhou, T. Naka, Q. Wei, J.-G. Mao, G.-C. Guo, J.-S. Huang. *Inorg. Chem.*, **42**, 2136 (2003).

[14] Y.-H. Wen, X.-L. Xie, L. Wang. *J. Coord. Chem.*, **64**, 459 (2011).
[15] G.M. Sheldrick. *Acta Crystallogr.*, **A64**, 112 (2008).
[16] A.J.C. Wilson. *International Tables for X-ray Crystallography*, Vol. C, Kluwer Academic Publishers, Dordrecht (1992) (Tables 6.1.1.4 (pp. 500–520) and 4.2.6.8 (pp. 219–222), respectively).
[17] K. Nakamoto. *Infrared and Raman Spectra of Inorganic and Coordination Compounds*, 4th Edn, Wiley-Interscience, New York (1986).
[18] S.-M. Yue, H.-B. Xu, J.-F. Ma, Z.-M. Su, Y.-H. Kan, H.-J. Zhang. *Polyhedron*, **25**, 635 (2006).
[19] S.-G. Liu, J.-L. Zuo, Y.-Z. Li, X.-Z. You. *J. Mol. Struct.*, **705**, 153 (2004).
[20] C.J. Matthews, W. Clegg, S.L. Heath, N.C. Martin, M.N.S. Hill, J.C. Lockhart. *Inorg. Chem.*, **37**, 199 (1998).
[21] T. Li, X. Su, Y. Xiu, X.-R. Meng. *J. Coord. Chem.*, **65**, 1792 (2012).
[22] W.J. Geary. *Coord. Chem. Rev.*, **7**, 81 (1971).
[23] E.C. Long, J.K. Barton. *Acc. Chem. Res.*, **23**, 271 (1990).
[24] B.C. Baguley, M. Le Bret. *Biochemistry*, **23**, 937 (1984).
[25] H.-L. Wu, K.-T. Wang, F. Kou, F. Jia, B. Liu, J.-K. Yuan, Y. Bai. *J. Coord. Chem.*, **64**, 2676 (2011).
[26] H.-L. Wu, K.-T. Wang, F. Jia, B. Liu, F. Kou, J.-K. Yuan, J. Kong. *J. Coord. Chem.*, **63**, 4113 (2010).
[27] C. Gao, X. Ma, J. Tian, D. Li, S. Yan. *J. Coord. Chem.*, **63**, 115 (2010).
[28] W. Li, C.-H. Li, Y.-Q. Yang, Z.-M. Chen, Y. Wang. *Chin. J. Inorg. Chem.*, **24**, 1360 (2008).
[29] M.T. Carter, M. Rodriguez, A.J. Bard. *J. Am. Chem. Soc.*, **111**, 8901 (1989).
[30] X.L. Wang, H. Chao, H. Li, X.L. Hong, L.N. Ji, X.Y. Li. *J. Inorg. Biochem.*, **98**, 423 (2004).
[31] Y. Kou, J. Tian, D. Li, W. Gu, X. Liu, S. Yan, D. Liao, P. Cheng. *Dalton Trans.*, 2374 (2009).
[32] G.-Y. Xu, K. Jiao, Y.-T. Li, Y. Ren, X.-Z. Zhang. *Chem. J. Chinese U.*, **28**, 49 (2007).
[33] A.J. Bard, L.R. Faulkner. *Electrochemical Methods: Fundamentals and Applications*, 2nd Edn, John Wiley & Sons Inc., New York (2001).
[34] E. Laviron. *J. Electroanal. Chem.*, **52**, 355 (1974).
[35] L.-Y. Zhang, J.-P. Zhang, Y.-Y. Lin, X.-M. Chen. *Cryst. Growth Des.*, **6**, 1684 (2006).
[36] Z.W. Wang, C.C. Ji, J. Ji, Z.J. Guo, Y.Z. Li, H.G. Zheng. *Cryst. Growth Des.*, **9**, 475 (2009).
[37] X.-L. Wang, J.-X. Zhang, L.-L. Hou, G.-C. Liu, H.-Y. Lin, A.-X. Tian. *J. Coord. Chem.*, **64**, 1177 (2011).
[38] R. Wang, D. Yuan, F. Jiang, L. Han, Y. Gong, M. Hong. *Cryst. Growth Des.*, **6**, 1351 (2006).